scientific reports

Check for updates

OPEN

Magnetic hyperthermia therapy enhances the chemoradiosensitivity of glioblastoma

Daniel Rivera[1,2,3,8], Alexandros Bouras[1,2,3,8], Milena Mattioli[1,2], Maria Anastasiadou[3], Anna Chiara Pacentra[1,2], Olivia Pelcher[1,2], Corrine Koziel[1,2], Alexander J. Schupper[3], Tori Chanenchuk[3], Hayden Carlton[4], Robert Ivkov[4,5,6,7] & Constantinos G. Hadjipanayis[1,2,3]✉

Glioblastoma (GBM) is the most common primary brain cancer and is resistant to standard-of-care chemoradiation therapy (CRT). Magnetic hyperthermia therapy (MHT) exposes magnetic iron oxide nanoparticles (MIONPs) to an alternating magnetic field (AMF) to generate local hyperthermia. This study evaluated MHT-mediated enhancement of CRT in preclinical GBM models. Cell viability and apoptosis were assessed in GBM cell lines after water bath heating with radiation and/or temozolomide. Heating efficiency of MIONPs after intracranial delivery was measured in healthy mice. MHT with CRT was performed in syngeneic and patient-derived xenograft (PDX) GBM tumors. Tissue sections were analyzed for γ-H2AX, HSP90, CD4+T cells, and microglial cells. Tumor burden and survival were assessed. Hyperthermia with radiation and temozolomide significantly reduced cell viability and increased apoptosis. Hyperthermia predominantly exhibited additive to synergistic interactions with both treatment modalities and reduced doses needed for tumor cell growth inhibition. In vivo, MHT with CRT decreased tumor burden and increased survival in PDX and syngeneic models. Immunohistochemistry showed increased γ-H2AX, HSP90, microglial activation, and CD4+T cells after MHT in combination with CRT. Overall, adjuvant hyperthermia enhances CRT efficacy in GBM cells, with MHT improving survival outcomes in rodents. Sufficient intracranial heating and MIONP retention for repeated treatments was achieved, supporting further clinical translation.

Keywords Glioblastoma, Magnetic hyperthermia therapy, Magnetic iron-oxide nanoparticles, Radiation therapy, Temozolomide, Chemoradiation

Glioblastoma (GBM), a World Health Organization (WHO) grade IV glioma, is an aggressive and incurable form of primary brain cancer with a poor prognosis[1]. GBM is characterized by diffuse invasive growth into surrounding brain tissue and therapy resistance, leading to treatment failure and inevitable local recurrence[2]. Current standard-of-care treatment consists of maximal, safe tumor resection with fractionated radiation therapy (RT) and concurrent and adjuvant temozolomide (TMZ) chemotherapy, collectively known as chemoradiation (CRT)[3]. However, GBM remains fatal due to the inability to completely resect tumor that has infiltrated into surrounding regions of the brain, drug delivery challenges across the blood-brain barrier (BBB), tumor heterogeneity, and the multiple methods in which GBM adapts to resist modern therapies[4–6]. Despite substantial progress, standard of care continues to achieve a median survival time of only 15–18 months from time of diagnosis, indicating an urgent need for novel and more effective treatments[7]. Sensitizing GBM tumors to CRT may provide a better approach for future GBM treatment.

[1]Brain Tumor Nanotechnology Laboratory, UPMC Hillman Cancer Center, Pittsburgh, PA, USA. [2]Department of Neurological Surgery, University of Pittsburgh, 200 Lothrop Street, Suite F-158, Pittsburgh, PA 15213, USA. [3]Department of Neurological Surgery, Icahn School of Medicine at Mount Sinai, New York City, NY, USA. [4]Department of Radiation Oncology and Molecular Radiation Sciences, Johns Hopkins University School of Medicine, Baltimore, MD, USA. [5]Department Oncology, Sydney Kimmel Comprehensive Cancer Center, Johns Hopkins University School of Medicine, Baltimore, MD, USA. [6]Department of Mechanical Engineering, Whiting School of Engineering, Johns Hopkins University, Baltimore, MD 21218, USA. [7]Department of Materials Science and Engineering, Whiting School of Engineering, Johns Hopkins University, Baltimore, MD 21218, USA. [8]Daniel Rivera and Alexandros Bouras contributed equally to this work. ✉email: hadjipanayiscg2@upmc.edu

Magnetic hyperthermia therapy (MHT) is a treatment approach in which a safe, external alternating magnetic field (AMF) is applied to induce heating of locally delivered magnetic nanoparticles (MNPs)[8,9]. Magnetic iron-oxide nanoparticles (MIONPs) are often used for MHT because they have excellent heating capabilities, established biocompatibility, and dual functionality as therapeutic and diagnostic imaging agents[10,11]. Heating tumor tissue between 40 and 45 ºC for a duration of 15 to 60 min decreases cancer cell viability, radiosensitizes tumor cells, promotes anti-tumor immune signaling, and increases intratumoral blood flow for improved drug delivery[12–15].

Unlike other heat-based therapies used to treat GBM, MHT can be repeated in multiple sessions non-invasively in the postoperative setting. since MIONPs remain near the delivery site for weeks to months, and the low frequency AMFs penetrate through skin and bone with little attenuation to reach deep-seated intracranial tumors[16,17]. Safety and efficacy of MIONP-mediated MHT of GBM in both preclinical and clinical studies resulted in its approval in 2010 by the European Medicines Agency to treat recurrent GBM with MHT in combination with fractionated RT[18–20]. In those early clinical studies of MHT in GBM patients, high concentrations of MIONPs were required to generate effective local hyperthermia. In addition, no prior studies have investigated MHT in combination with adjuvant CRT for GBM.

The objective of this study was to determine if adjuvant MHT enhances the anti-tumor effects of CRT in patient-derived and murine GBM models. Hyperthermia (HT) in combination with ionizing radiation (IR) and/or TMZ was evaluated in cell culture studies utilizing both new and recurrent therapy-resistant GBM cells. After establishing a rodent model for reproducible and effective intracranial MHT in several sessions, alterations to the tumor microenvironment and combination therapy efficacy were assessed in both syngeneic and patient-derived xenograft (PDX) GBM tumors. A single intracranial administration of MIONPs was performed using convection-enhanced delivery (CED)[21].

Results
Chemoradiation enhancement of GBM cells by hyperthermia
Cell viability studies
Across SD3, G-16,302, and GL-261 cell lines, HT significantly reduced cell viability compared to untreated controls, with HT + TMZ + IR producing the greatest decrease in viability (Fig. 1A–C). In SD3 and GL-261 cells, adding HT to TMZ, IR, or TMZ + IR decreased cell viability significantly more ($P \leq 0.0001$) than TMZ, IR, or TMZ + IR alone. Clonogenic assays of GL-261 cells corroborated these findings (Fig. 1D). No surviving colonies were observed in the triple-agent group, despite having the highest initial seeding density (1×10^4 cells). G-16,302 cells showed a more modest response following exposure. While there was a statistically detectable difference between the HT and HT + TMZ + IR groups ($0.01 \leq P \leq 0.05$), the magnitude of this difference was smaller than those measured in SD3 and GL-261 cells.

Annexin V/propidium iodide analysis
AnnexinV/Propidium Iodide staining, and flow cytometry analysis revealed changes in cell populations for both SD3 and GL-261 cell lines following exposure to HT, IR and/or TMZ. The triple-agent combination resulted in a higher percentage of AnnexinV and/or Propidium Iodide positive cells compared to untreated controls, HT alone, and TMZ + IR groups at 4-hours and 24-hours post-exposure in SD3 cells. For GL-261 cells, this increased positive staining in the triple-agent group compared to all other groups was observed only at 24 h post-treatment (Fig. 1E–H). Results for additional treatment groups (IR, TMZ, HT + IR, HT + TMZ) are presented in supplementary Fig. 1.

Evaluating the combination interactions of hyperthermia with chemoradiation
In GL-261 cells, the combination interactions between low-dose HT and escalating doses of IR were found to be predominantly additive with evidence of slight synergy at certain dose combinations (4 Gy, CI = 0.87). Analysis of dose reduction indices (DRI) revealed consistent dose-sparing effects, with values ranging from 2.62 at 2 Gy to 1.39 at 8 Gy. (Fig. 2, A). HT combined with TMZ demonstrated a dose-dependent interaction profile, with synergistic effects observed at lower TMZ concentrations (12.5–25 µm, CI = 0.82–0.88), transitioning to antagonism at higher concentrations (50–100 µm, CI = 1.13–1.73). The DRI values correspondingly decreased from 4.82 at 12.5 µm to 0.79 at 100 µm (Fig. 2B). Our analysis of SD3 cells revealed a dose-dependent interaction between HT and IR, with a transition from synergistic effects at low radiation doses (3 Gy, CI = 0.78) to additive effects at higher doses (5–10 Gy, CI 0.91–1.03), accompanied by DRI values ranging from 4.37 at 3 Gy to 1.80 at 10 Gy (Fig. 2C). Furthermore, in the highly TMZ-sensitive SD3 cell line, we observed a complex interaction pattern between HT and TMZ. The combination demonstrated slight synergism at 1 µm TMZ (CI = 0.87), transitioned to slight antagonism and near-additive effects at 3 µm and 6 µm (CI = 1.13, 1.02), and showed the strongest synergism at 9 µm (CI = 0.73). DRI values remained greater than 1 across all TMZ doses (ranging from 2.35 at 1 µm to 1.81 at 9 µm) (Fig. 2D). CI values were interpreted based on guidelines provided by Chou et al.[22] (Fig. 2E).

Optimization of intracranial MHT in healthy mice
MIONP dosing and heating characterization
MIONP heating was found to positively correlate with the mass of iron in the sample as well as AMF field frequency and amplitude. SLP ranged from 92.66 +/- 13.55 W/g at the lowest field parameter (4.8 kA/m, 341.5 kHz) to 448 +/- 22.43 W/g at the highest field parameter (11.1 kA/m, 341.5 kHz) (supplementary Fig. 2).
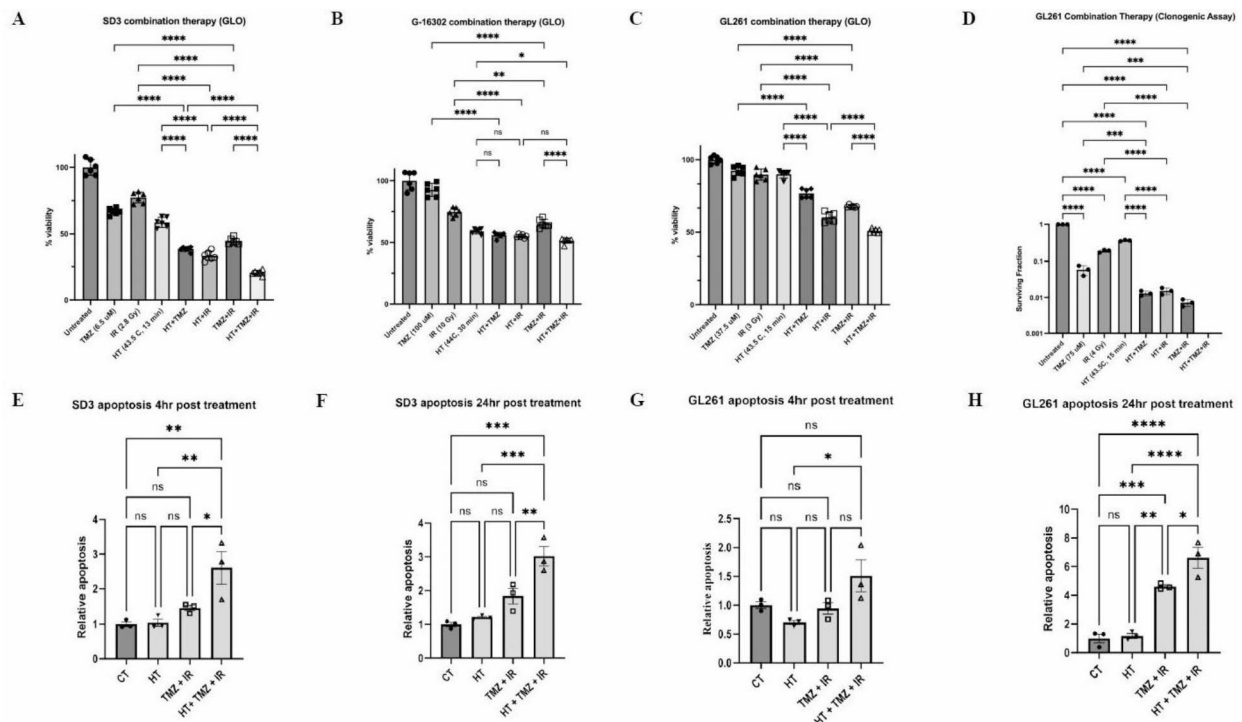
Fig. 1. Hyperthermia enhances TMZ and IR antitumor effects leading to decreased tumor cell viability and increased apoptosis. CellTiter GLO viability assay of SD3 (**A**), G-16,302 (**B**), and GL261 (**C**) was performed following treatment with water bath HT, TMZ, and/or IR and normalized to untreated controls. A clonogenic survival assay of GL261 cells (**D**) was performed following the same treatment conditions. In all instances, the addition of HT to TMZ and/or IR decreased viability by a greater extent than IR or TMZ monotherapy (**** $P < 0.0001$, one-way ANOVA and Tukey's multiple comparisons test). Three separate trials were performed per experiment, and for each experiment six technical replicates were used per group. Apoptosis of GBM cell lines after 4–24 h of HT, TMZ + IR or HT + TMZ + IR treatment determined by AnnexinV/Propidium iodide staining and Flow Cytometry analysis on SD3 (**E**, **F**) and GL261 (**G**, **H**) cell lines. Apoptosis values of the treated cells were normalized to the baseline of untreated cell values (CT). Results are expressed as mean values ± SEM. Statistical significance was determined using one-way ANOVA test with Tukey's multiple comparisons adjustment : $p < 0.0001$ ****, $p = 0.0001$ ***; $p < 0.001$ **, $p < 0.01$*.

Intracranial temperature measurements
A visual representation of rodent intracranial MHT and temperature measurements is provided in Fig. 3. As expected, measured temperatures correlated with the overall mass of MIONPs injected intracranially (Fig. 4A–D). Exposing brains of mice injected with 10 µL of 80 mg/mL MIONPs to the AMFs generated the highest measured intracranial T_{max} of 50.7 ± 0.2 °C compared to an average T_{max} of 45.3 ± 0.2 °C (8 µL, 80 mg/mL), 38.0 ± 0.2 °C (8 µL, 60 mg/mL), and 30.7 ± 0.2 °C (8 µL, 40 mg/mL) (Fig. 4A–D). Additionally, hyperthermic intracranial temperatures were measured during heating trials performed 24 and 48 h post CED (8 µL, 80 mg/mL), with mean T_{max} of 42.0 ± 0.2 °C and 41.8 ± 0.2 °C, respectively (Fig. 4E, F). 8 µL of 80 mg/mL was used for subsequent studies based on animal tolerability in conjunction with efficient intracranial MIONP heating.

Evaluation of MHT with CRT combination therapy efficacy in GBM rodent models
Syngeneic GL-261 mouse model
Tumor burden assessment
Figure 5A shows the treatment scheme and timeline. GL-261-LUC tumor generation was confirmed by MRI and Hematoxylin & Eosin (H&E) staining (Fig. 5B, C). Staining revealed densely cellular cords, scant fibrovascular stroma, rare nuclear palisading, multifocal necrosis, hemorrhage, and vascular clusters associated with necrosis or normal tissue (Fig. 5D). Prussian blue staining 24 h post-CED showed MIONP distribution intra- and peritumorally (Fig. 5E). Representative BLI images are shown in Fig. 5F. Serial BLI at 6-, 14-, and 17-days post-implantation measured total flux to monitor tumor progression (Fig. 5G, H). All treatments reduced tumor burden, with MHT + CRT showing the most significant decrease compared to all groups and was associated with increased survival (Fig. 5I).

Survival analysis
The MHT + CRT combination therapy resulted in improved survival outcomes compared to MHT or CRT alone in tumor-bearing mice. By the pre-determined study endpoint of 66 d post tumor implantation, only one
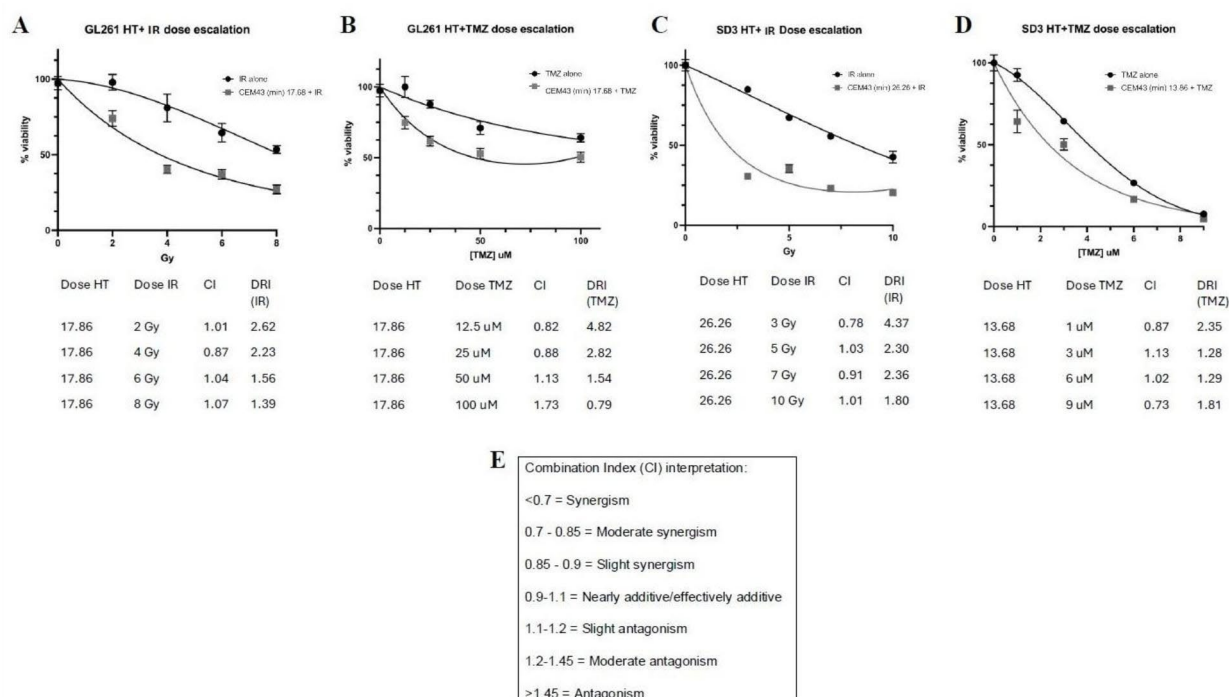
Fig. 2. Hyperthermia promotes synergistic and additive effects with radiation and temozolomide in GL261 and SD3 GBM cell lines. Cell viability curves showing the effects of escalating doses of ionizing radiation (IR) or temozolomide (TMZ) alone (black circles) or in combination with hyperthermia (HT) pretreatment (gray squares) in GL261 (A, B) and SD3 (C, D) GBM cell lines. HT doses are represented in terms of thermal dose at cumulative equivalent minutes at 43 C (CEM43). (**A**) GL261 cells treated with 17.86 min HT combined with escalating RT doses (2–8 Gy). (**B**) GL261 cells treated with 17.86 min HT combined with escalating TMZ doses (12.5–100 μM). (**C**) SD3 cells treated with 26.26 min HT combined with escalating RT doses (3–10 Gy). (**D**) SD3 cells treated with 13.68 min HT combined with escalating TMZ doses (1–9 μM). Tabulated values below each graph show the combination index (CI) and dose reduction index (DRI) for each combination. Separate HT monotherapy dose escalation studies were performed simultaneously (data not shown) to determine CI. Per Chou T.C. et al. (2006), CI values are interpreted as indicated in the included textbox (**E**). Dose reduction index (DRI) values represent the fold reduction in dose required when using the combination to achieve the same effect as the single agent alone. Error bars represent standard error of the mean.
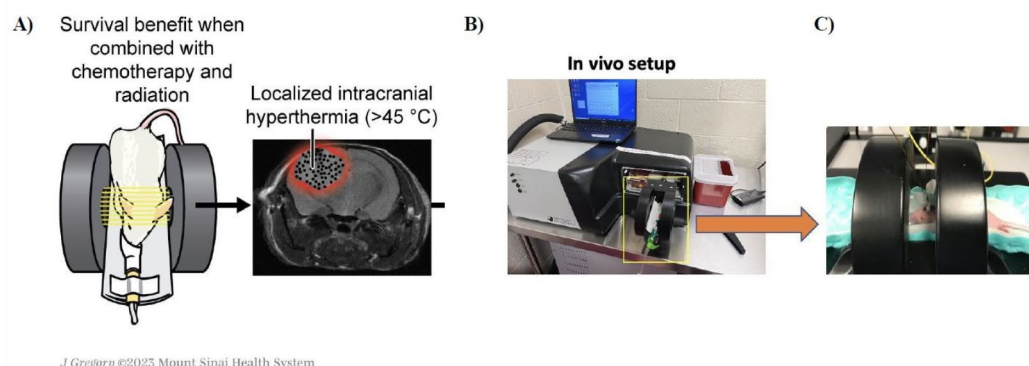

Fig. 3. Visual representation of rodent intracranial MHT. (**A**) Graphic representation of preclinical rodent intracranial MHT, illustrating localization of magnetic iron oxide nanoparticles within the tumor area. (**B**) Actual experimental setup for in vivo MHT. (**C**) Photograph showing representative intracranial temperature measurement experiment, with temperature probes inserted through surgically implanted guide cannulas on the skull surface.
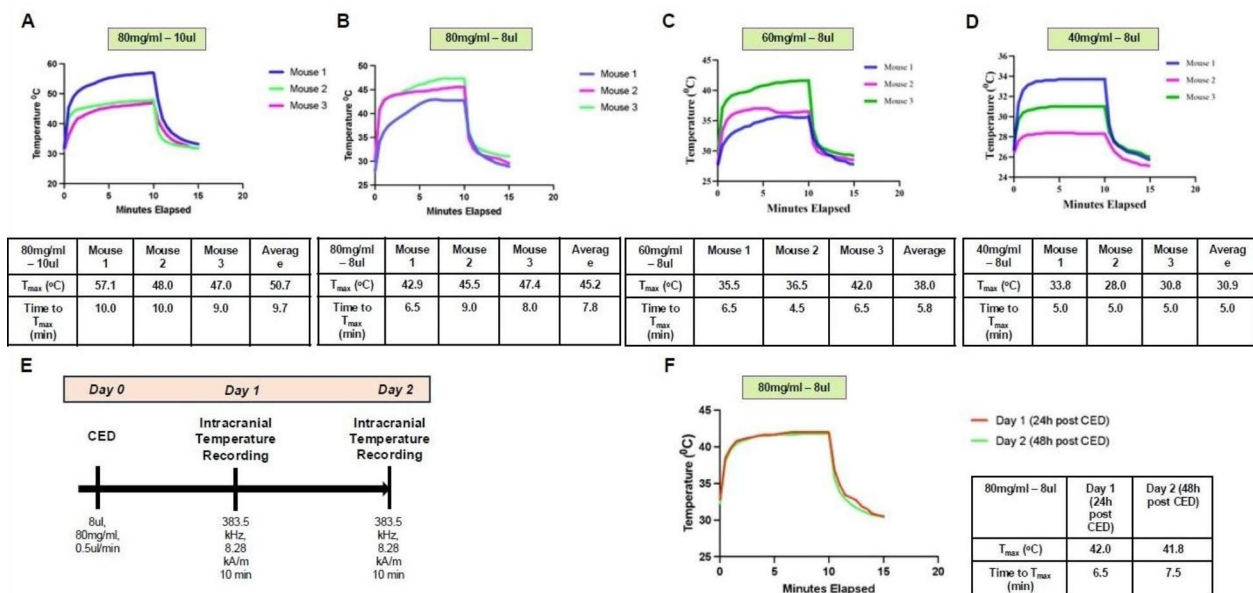
Fig. 4. MIONP concentration and AMF conditions determine temperature of intracranial heating in mice. A–D Healthy mice ($n = 3$) were exposed to an external AMF (383.5 kHz, 8.28kA/m) and intracranial temperature measurements were recorded immediately post-delivery of MIONPs by convection-enhanced delivery (CED) for a total of 15 min (AMF ON for 10 min and AMF OFF for 5 min). Mice underwent CED of MIONPs with (**A**) 80 mg/ml at 10ul, (**B**) 80 mg/ml at 8ul, (**C**) 60 mg/ml at 8ul and (**D**) 40 mg/ml at 8ul. (**E**) To replicate the therapeutic MHT + CRT scheme, temperature measurements were performed 24 h and 48 h post-CED (80 mg/ml, 8ul, 0.5ul/min) for a total of 15 min (AMF ON for 10 min and AMF OFF for 5 min) on the same mouse ($n = 1$). (**F**) Temperature measurement results showing repeated MIONPs heating 24 h and 48 h post CED in the same mouse brain.

mouse remained alive - from the MHT + CRT group. Necropsy of this surviving mouse confirmed the continued presence of intracranial MIONPs. All animals in the other treatment groups (control, MHT alone, and CRT alone) had died before this endpoint. Median survival times were as follows: control (18 d), MHT alone (17 d), CRT alone (21 d), and MHT + CRT (38 d) (Fig. 5I).

Patient-derived xenograft (PDX) SD3 model

Tumor characterization
A treatment scheme and timeline of the survival study is provided in Fig. 6A. SD3 xenograft generation was confirmed by MRI and H&E staining at 32 days post-implantation (Fig. 6B, C). The cells were polygonal with moderate eosinophilic cytoplasm. Multifocal nests of neoplastic cells were present in adjacent neuroparenchyma. Mild, multifocal hemorrhage at the mass periphery extended into adjacent neuroparenchyma. The tumor mass infiltrated and compressed the nearby tissue (Fig. 6C). Additional PB staining of mouse brain sections revealed intratumoral and peritumoral MIONP distribution 24 h post-CED (Fig. 6D).

Survival analysis
A survival benefit was observed in the MHT in combination with CRT treated animals when compared to untreated control, MIONP, MHT, and CRT animal groups (Fig. 6E). Six out of ten mice (60%) in the CRT group and nine out of ten mice (90%) of the MHT + CRT group were alive at 66 d, the study endpoint.

Analysis of tumor microenvironment following MHT in combination with CRT
The treatment scheme and timeline of the immunostaining study is provided in Figs. 7A and 8A.

DNA damage response
Statistically significant increases in γ-H2AX foci were observed in GL-261 tumors treated with MHT + CRT combination therapy compared to either CRT ($P < 0.05$) or untreated controls ($P < 0.005$) (Fig. 7B).
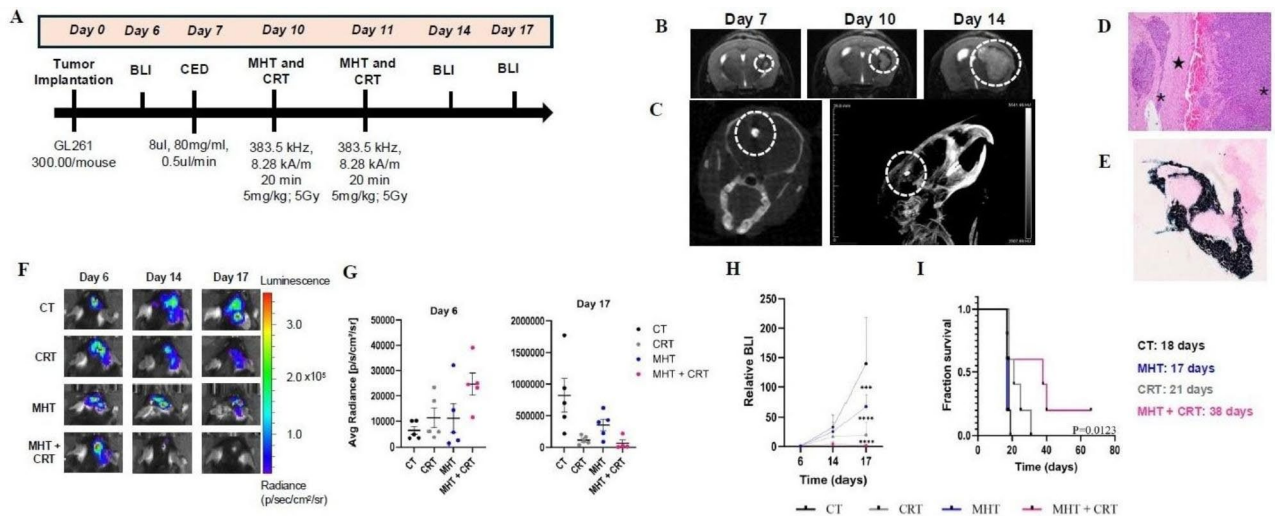
Fig. 5. MHT in combination with fractionated RT reduces viable tumor volume measured by BLI and increases overall survival in syngeneic rodent GL-261 glioma tumors (3×10^5 cells/mouse). (**A**) Therapeutic scheme used for untreated controls (CT), fractionated CRT (5 mg/kg TMZ x2 + 5 Gy x2), MHT (MIONPs 80 mg/ml, 8ul + AMF 383.55 kHz, 8.28kA/m, 20 min) and MHT + CRT. (**B**) Representative MRI (T2WI) images showing infiltrative GBM tumors 7-, 10- and 14-days post tumor cell implantation in the control group (dotted circle). (**C**) Representative CT scan images showing MIONPs (dotted circle) in the brain in MHT and MHT + CRT group. (**D**) H & E staining of intracranial GBM tumor formation (magnification 100X) * = tumor core (right) and infiltrative area (left), star = normal brain tissue. (**E**) Prussian Blue staining of mouse brain section revealing intratumoral distribution of MIONPs 24 h post CED (magnification 40X). (**F**) Representative BLI images of CT, CRT, MHT and MHT + CRT mice groups on days 6, 14 and 17 post tumor implantation. (**G**) Tumor growth/inhibition at Day 6 (before treatment) and day 17 (6 days after treatment end). Data are expressed as average radiance values ± SEM. (**H**) Time course quantification of tumor BLI signals in the 4 treatment groups ($n = 5$). Results are expressed as the mean of radiance values ± SD detected at the indicated time points. P-values are calculated using two-way ANOVA and Tukey's multiple comparison test (** $P = 0.02$; **** $P < 0.0001$). (I) Kaplan-Meier survival curve ($n = 5$ per group) and median survival days. P-values are calculated using Log-Rank Mantel Cox test.

Heat shock response
HSP90 expression was found to be significantly elevated in the treated hemispheres of MHT + CRT combination therapy treated mice compared to either CRT ($P < 0.05$) or untreated controls ($P < 0.05$) (Fig. 7C). Neither γ-H2AX nor HSP90 levels were found to be elevated in the CRT alone group compared to untreated controls.

Immune cell recruitment
CD4 signal was found to be elevated in the MHT + CRT group compared to either CRT or untreated control groups ($P < 0.05$), while no difference in CD8 signal intensity was found between any of the groups (Fig. 8B). Further analysis of the CD4 + population in the MHT with CRT combination therapy group revealed weak positivity for CD25. Foxp3 was found to be negative (data not shown).

Microglial activation
IBA-1 expression was found to be significantly higher in the MHT + CRT group compared to CRT ($P < 0.0005$) and untreated control groups ($P < 0.005$) (Fig. 8C). For all markers of immune cell recruitment, no difference was found between CRT and untreated controls.

Discussion
Effective GBM management requires novel therapies that can treat tumors in a durable fashion without toxicity to the surrounding brain. MHT has emerged as a promising treatment modality, allowing for multiple sessions of non-invasive, localized HT following a single administration of MIONPs[23,24]. Prior studies have shown the potential for MHT to enhance the anti-tumor effects of RT in human recurrent GBM patients utilizing early
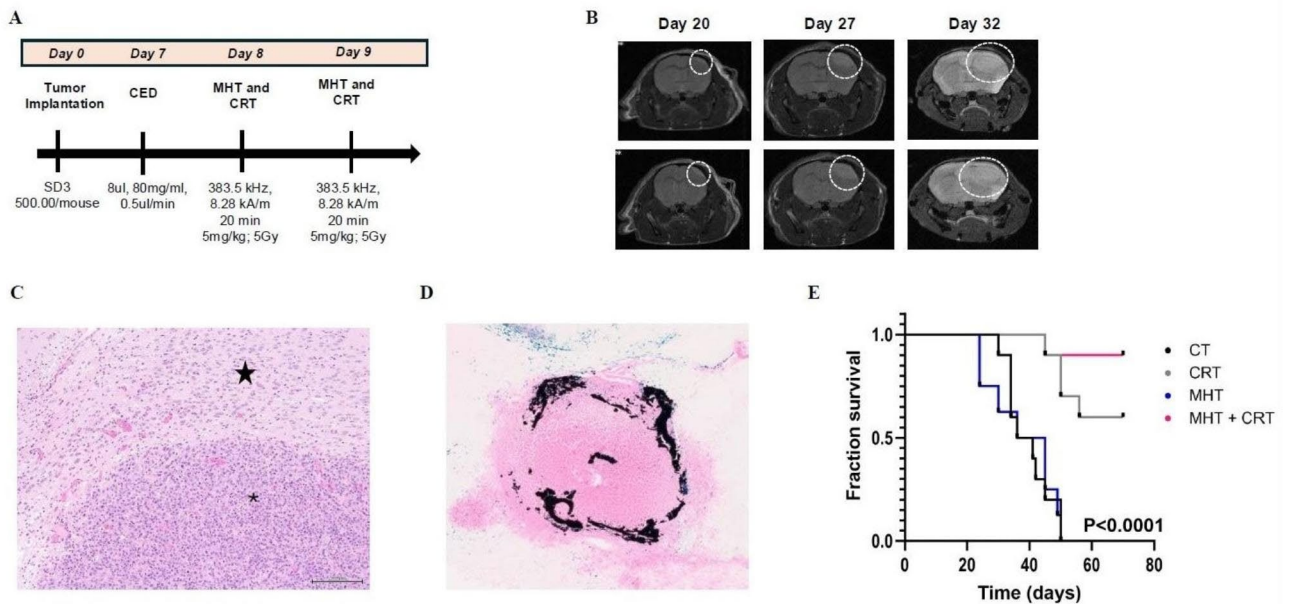
Fig. 6. MHT combined with CRT increases tumor response over single agent treatments in orthotopic SD3 human GBM tumors (5×10^5 cells/mouse). (**A**) Therapeutic scheme used for untreated controls (CT), fractionated CRT (5 mg/kg TMZ x2 + 5 Gy x2), MHT (MIONPs 80 mg/ml, 8ul + AMF 383.55 kHz, 8.28kA/m, 20 min) and MHT + CRT. (**B**) Representative MRI (T2WI) images showing infiltrative GBM xenografts 20-, 27- and 32-days post tumor cell implantation in the untreated control group (dotted circle). (**C**) H&E staining of intracranial GBM xenograft confirms tumor formation (magnification 100X) * = tumor core, star = normal brain tissue. (**D**) Prussian Blue staining of mouse brain section revealing intratumoral distribution of MIONPs 24 h post CED (magnification 40X). (**E**) Kaplan-Meier survival curve. P-value is calculated using the Gehan-Breslow Wilcoxon test.

generation MIONPs at high concentrations[18]. In our current study, we introduce a new formulation of nanoflower MIONPs (Synomag*) that provide therapeutic hyperthermia at low amplitude field requiring concentrations (< 20 mg/g/tissue) much lower than prior studies (> 50 mg/g/tissue).[18,25] These newer generation MIONPs also serve as tracers for magnetic particle imaging (MPI)[26]. The combination of MHT with CRT has not been well studied in preclinical GBM models. We sought to better understand the effects of HT in combination with CRT in multiple new and recurrent GBM cells and characterize the tumor microenvironment after MHT and/or CRT in both orthotopic syngeneic and PDX rodent glioma models.

In our cell culture studies, exposing cells to HT, TMZ, and/or IR confirmed that HT enhanced the anti-proliferative effects of TMZ and IR in primary GSCs (SD3), recurrent metastatic human GBM (G-16302), and murine GBM (GL-261) cell lines. Cell viability assays (Fig. 1A–C) and clonogenic survival studies (Fig. 1D) showed significant decreases in cell viability and colony formation when cells were exposed to HT with either TMZ and/or IR, compared to TMZ and/or IR alone. Interestingly, while response to triple-agent exposure in recurrent metastatic (G-16302) and murine (GL-261) GBM cells was comparable at about 50% as measured by the GLO viability assay, the clonogenic survival assay revealed a more dramatic reduction in clonogenic survival for GL-261, with no detectable colonies under the same treatment. This difference reflects the distinct biological processes each assay measures and their respective time-to-read results. The clonogenic assay captures long-term proliferative capacity as the read-out occurs after several cell replication cycles, whereas the GLO assay detects metabolic activity at a shorter time point. The higher viability observed in GLO is therefore likely due to the detection of metabolically active cells for which full effects of DNA damage have yet to manifest.

Following these initial experiments, we sought to characterize whether the observed enhancement was synergistic, additive, or antagonistic by determining combination indices (CI) and dose reduction indices (DRI) for HT combined with escalating doses of either TMZ or IR in the GL-261 and SD3 tumor cell lines. Our findings demonstrated that hyperthermia predominantly exhibited additive to synergistic interactions with both treatment modalities, though variations occurred depending on dose and cell line. The apparent antagonism observed at higher TMZ concentrations (50–100 µM) in GL261 cells likely reflects a saturation effect rather than true biological antagonism, as these concentrations approach our experimentally determined maximum effective dose of TMZ where cell killing plateaus regardless of additional drug concentration. This phenomenon can artificially inflate CI values while masking the actual benefit of combination therapy. From a clinical translation perspective, the dose reduction indices are particularly significant, with DRI values consistently
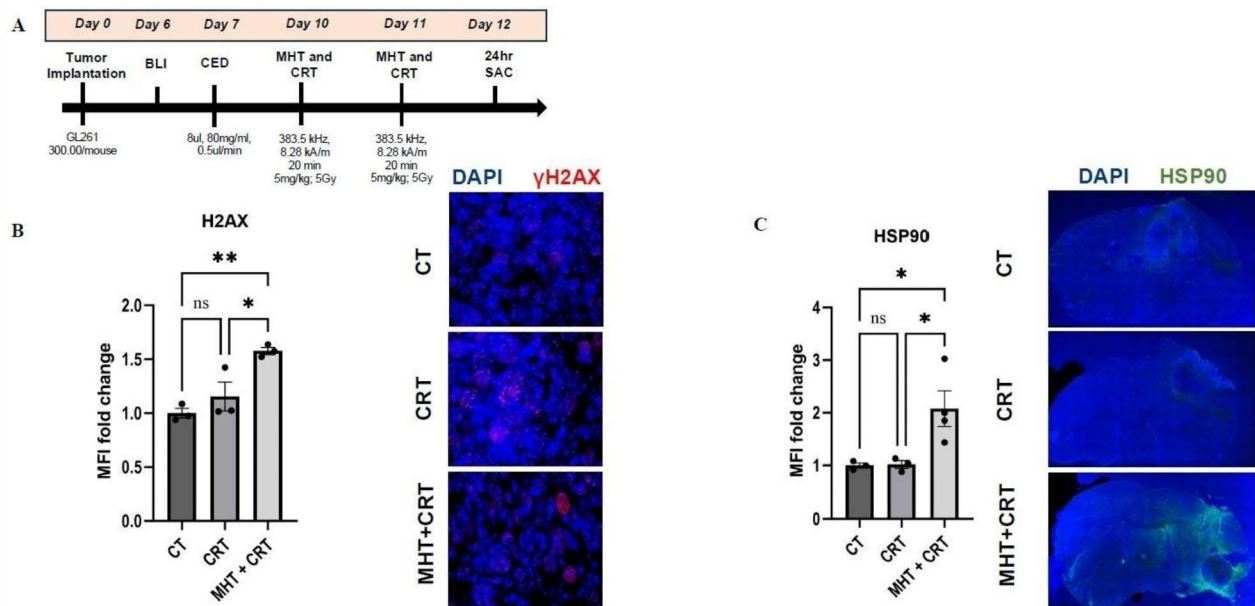
Fig. 7. MHT combined with CRT increases markers of DNA damage and heat-shock response. (**A**) Therapeutic scheme used for immunostaining after MHT with CRT in syngeneic rodent GL-261 GBM tumors (3×10^5 cells/mouse). Representative images and quantification of immunostaining for γ-H2AX in the tumor core (**B**), and HSP90 in the tumor hemisphere (**C**) 24 h after the last CRT (fractionated RT, 5Gy ×2, and TMZ, 5 mg/kg × 2) or MHT (8 uL, 80 mg/mL, 0.5 uL/min MIONP CED, 383.55 kHz, 8.28 kA/m, 20 min AMF) with CRT, and from untreated controls (CT). Data represent mean ± SEM. Statistical significance was determined using one-way ANOVA test with Tukey's multiple comparisons adjustment, ns = Not significant, $p < 0.05 =$ *, $p < 0.005 =$ **.

above 1 for most treatment combinations, indicating substantial dose-sparing potential. These findings are in line with previous work demonstrating that HT can reduce the required dose of RT to achieve antitumor effect comparable with RT alone[27]. The inverse relationship between DRI and increasing doses of TMZ or IR suggests that hyperthermia may provide its greatest benefit in allowing meaningful dose reductions at lower treatment intensities. This pattern could reflect hyperthermia's mechanism of action in sensitizing cells to initial therapeutic insult. Alternatively, this relationship could be explained by the fact that at higher monotherapy doses where TMZ and IR are capable of potent cell-killing on their own, there is less room for the combination therapy to show further benefit in our in vitro model.

Flow cytometry analysis using Annexin V and Propidium Iodide staining showed an increased proportion of positively stained SD3 cells at 4- and 24-hours post-exposure, and of GL-261 cells only at 24 h, when HT was added to TMZ + IR (Fig. 1E-H). This observation suggests increased cell death, potentially via apoptosis, although further studies using additional apoptosis detection methods are needed to confirm specific mechanisms involved in the enhanced efficacy of the combination therapy. Notably, while HT or TMZ + IR individually reduced cell viability in CellTiter GLO assays, neither significantly increased early apoptosis, with only minor increases after TMZ + IR in GL-261 cells at 24 h. This discrepancy suggests that HT or TMZ + IR individually may induce different cell stress responses without triggering immediate apoptosis.

The effects of IR on cell replication are slow to manifest, with time-dependent variability as individual cells attempt to repair DNA damage[28]. The increased Annexin V/PI positive staining in the triple-agent combination group at earlier time points suggests a potentially accelerated cellular response. Individually, HT and TMZ + IR act on different cell processes, with the former directly affecting protein structure and function, whereas the latter targets DNA. Our data suggest that together they may generate an effect that inhibits repair to overcome resistance or directly affects pathways involved in resistance mechanisms to produce more pronounced tumor cell death than either treatment alone.

Collectively, our in *vitro* results support that hyperthermia enhances the cytotoxic effects of TMZ and IR and may serve as a valuable adjunct therapy that could enable clinically meaningful dose reductions while maintaining therapeutic efficacy. This finding is significant, as previous clinical trials using MHT for GBM have focused on combining MHT with single-agent RT, with less attention to MHT combinations that include TMZ. Even the therapy-resistant GBM cell line (G-16302) exhibited sensitivity to moderate HT (44 °C for 30 min), suggesting inclusion of HT may be effective against recurrent GBM lines. However, G-16,302 displayed the most resistance to HT, indicating possible overlap in resistance pathways to TMZ, IR, and HT.
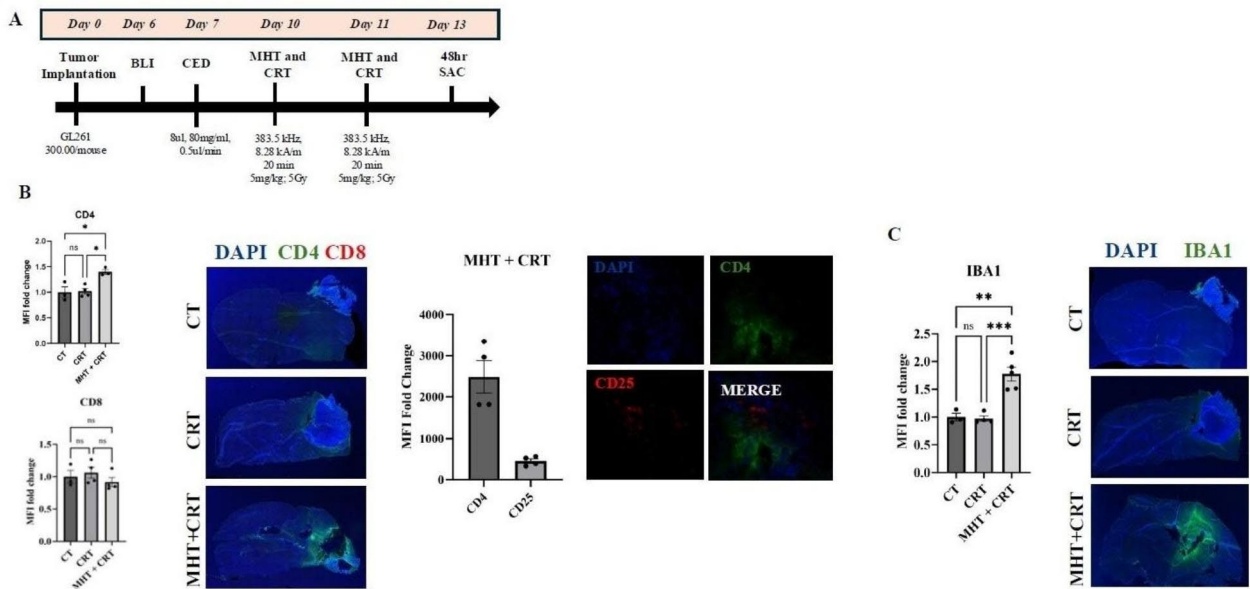
Fig. 8. MHT combined with CRT increases CD4 + cell recruitment and IBA-1 expression in the tumor microenvironment. (**A**) Therapeutic scheme used for immunostaining of biomarkers after MHT with CRT in syngeneic rodent GL-261 GBM tumors (300,000 cells/mouse). Representative images and quantification of immunostaining for CD4/CD25 (**B**), and IBA1 (**C**) 48 h post the last treatment of CRT (fractionated RT, 5 Gy x2, and TMZ, 5 mg/kg x 2) or MHT (8 uL, 80 mg/mL, 0.5 uL/min MIONP CED, 383.55 kHz, 8.28 kA/m, 20 min AMF) with CRT, and from untreated controls (CT). Data represent mean ± SEM. Statistical significance was determined using one-way ANOVA test with Tukey's multiple comparisons adjustment, ns = Not significant, $P < 0.05 = *$, $P < 0.005 = **$, $P < 0.0005 = ***$.

The observed enhancement arising from combining HT with TMZ and RT was also evident in orthotopic GBM rodent models. At 24 h post-treatment, tumor treated with MHT and CRT expressed elevated increased HSP90 expression, a key stress-response chaperone protein, compared to CRT alone and untreated controls. Taken together, these results indicate increased stress responses with evidence suggestive of increased numbers (and/or persistence) of DNA breaks in tumor cells exposed to the combined therapies. Interestingly, CRT did not exhibit elevated HSP90 expression compared to untreated controls. Although prior studies have shown that CRT can induce increased HSP90 expression 24 h after treatment[29], it is possible that the subtherapeutic chemotherapy dose used in our study did not generate enough proteotoxic stress to trigger HSP90 in this time frame[30]. Furthermore, HT is known to directly activate heat-shock factor 1, which is the primary regulator of HSP expression, and cause membrane damage, cytoskeletal disruption, and oxidative stress, all of which may explain the amplified the HSP response[31]. Moreover, HT-induced changes may alter HSP90's ability to stabilize oncoproteins and regulate stress responses[32], potentially enhancing cancer cell vulnerability to CRT-mediated tumor cell death. While HSP90 upregulation may indicate HT + CRT induced stress, HSP90 overexpression is also associated with tumor progression and development of thermal tolerance[33]. As a result, numerous studies have demonstrated the benefit of using HSP90 inhibitors in combination with HT and RT for treating GBM and other forms of cancer[34,35].

Additionally, γ-H2AX levels were increased 24 h after MHT and CRT combination therapy compared to CRT alone and untreated controls. Heat is known to inhibit DNA break repair, while radiation-exposed cells typically initiate repair quickly. The γ-H2AX signal we measured indicates conformationally stressed chromatin, signaling repair initiation, but does not directly measure repair kinetics. Increased γ-H2AX signal can also be generated directly by heat stress causing protein (i.e., histone) denaturation or conformational changes. From the data, whether the combination led directly to increased DNA damage or enabled DNA damage to persist by inhibiting repair is difficult to ascertain.

Our investigation of the tumor microenvironment revealed elevated numbers of CD4+ positive and IBA-1+ cells at 48 h after the addition of MHT to CRT. GBM is known for exhibiting an immunologically "cold" microenvironment, which contributes to its aggressiveness and resistance to immunotherapy. Increased presence of immune cells, particularly CD4+ T cells, within the tumor may indicate a shift towards a more immunologically active state, potentially enhancing anti-tumor responses. Our findings of weak CD25 positivity and FoxP3 negativity may indicate the transition of mature CD4 + CD25-Foxp3- precursors into adaptive or induced CD4 + CD25 + Foxp3 + regulatory T cells following MHT[36,37]. It is possible that by staining at 24 h post-

treatment, we captured this cell population in the midst of this change. This is an exciting result that may indicate immune response(s) to therapy-associated tissue damage enhanced tumor suppression; however, we measured no similar increases in CD8$^+$ T cells, and the presence of immune cells within the tumor alone is insufficient to conclude they are singularly inhibiting tumor growth. Furthermore, the absence of evidence of CD8 + T cell infiltration may be a consequence of general immune suppression in the brain designed to limit tissue damage associated with aggressive inflammation. Additional studies are needed to assess adaptive immune responses to combination therapy in GBM models to elucidate their role following MHT, and to assess their potential implications[38,39].

To further assess MHT's potential to enhance CRT in rodent GBM models, we conducted tumor burden and survival studies using orthotopic PDX and syngeneic mouse models. In the PDX survival study, while median survival could not be quantified due to high survival rates at the 66-day endpoint, nine out of ten mice in the MHT + CRT group survived compared to six out of ten in the CRT-only group, indicating a potential survival benefit. In the mouse GBM syngeneic model, the addition of MHT to CRT increased median survival by 17 days compared to CRT alone. Despite starting with the highest average tumor burden prior to treatment, the MHT + CRT cohort showed the greatest decrease in tumor size at the end of the study, as revealed by BLI. This reduction was more pronounced than in groups treated with either CRT or MHT alone. Notably, in the GBM syngeneic survival study, one mouse out of five treated with MHT + CRT survived until study conclusion. Necropsy of the brain from this individual revealed MIONPs remaining near the delivery site, demonstrating their persistence in the mouse brain for over 60 days after CED. This prolonged presence of MIONPs enables multiple MHT sessions after a single administration of MIONPs. Our pilot studies included only two MHT sessions, however the results motivate future studies exploring inclusion of additional MHT fractions with dose per fraction, total dose, and timing as study variables. It has been previously shown that increasing the number of MHT sessions correlates with greater tumor burden reduction in an orthotopic rat GBM model[40].

MHT has limitations, including challenges to simultaneously visualize MIONPs and measure thermal dose during treatment. MIONP temperature monitoring requires invasive intracranial probes, and their variable placement in mouse brains can yield misleading readings[41]. High MIONP concentrations create MRI artifacts, obscuring tissue anatomy. While we used CT scans to confirm MIONP localization, integrating a tracer modality, such as MPI with MHT shows promise (Supplementary Fig. 3) but needs development[42]. CED of MIONPs presents hurdles such as backflow and inadequate tissue penetration, leading to inhomogeneous distribution and suboptimal heating[43].

In summary, the addition of MHT enhanced the chemoradiosensitivity of GBM. This work represents one of the first studies investigating the potential therapeutic efficacy of MHT and CRT combinations in orthotopic GBM models and cell culture studies. Optimizing MHT timing and frequency could further enhance treatment efficacy, while the prolonged presence of MIONPs suggests the possibility of multiple MHT sessions over extended time-periods. Clinically, the ability to perform repeated, non-invasive MHT treatments following a single MIONP administration could offer significant advantages for treating residual, recurrent, or inoperable GBM tumors. The observed immune cell infiltration merits future investigation of combining MHT + CRT with immunotherapy. The thermal enhancement of IR and TMZ efficacy suggests potential for dose reduction, minimizing treatment-related toxicities. While further research is needed, our findings provide a strong rationale for pursuing clinical trials of MHT and CRT combination therapy in GBM patients.

Materials and methods
Protocol approval and adherence to relevant guidelines and regulations
All experiments received approval from the Institutional Animal Care Use Committee of Icahn School of Medicine at Mount Sinai and University of Pittsburgh School of Medicine. All experiments and methods were performed in accordance with the relevant guidelines and regulations outline by the ARRIVE guidelines (PLoS Bio 8(6), e1000412, 2010) as well as the American Veterinary Medical Association Guidelines for Euthanasia of Animals.

GBM cell lines and cell culture
The primary patient-derived GBM stem-cell line (GSC), SD3, and the recurrent metastatic GBM patient-derived cell line, G-16302, were obtained from Dr. Roland Friedel and Dr. Nadejda Tsankova of the Icahn School of Medicine at Mount Sinai. SD3 and G-16302 have been previously described[44–46]. GSCs are a population of highly tumorigenic self-renewing cells thought to be key drivers of disease progression, immune evasion, and recurrence despite treatment[47]. SD3 was cultured in supplemented NeuroCult™ NS-A Human basal medium (StemCell technologies, Vancouver, Canada). The established murine GBM cell line, GL-261 (American Type Culture Collection (ATCC, Manassas, VA), was transduced with MSCV-Luciferase retroviral particles to generate luciferase expressing cells (referred to as GL-261-LUC) for serial bioluminescence imaging (BLI) as previously described[48]. GL-261, GL-261-LUC, G-16302 were cultured in supplemented DMEM. Cell culture methods are described in greater detail in supplementary methods.

Animals and tumor implantation
Animals were housed in a facility with 12/12-hour light/dark cycles and access to food and water *ad libitum*. 6-8-week-old female outbred athymic nude mice homozygous for *Foxn1^{nu}* (Jackson Laboratory, Farmington, CT, USA) were implanted with 5×10^5 SD3 cells into right striatum (2 mm right lateral to bregma; 3 mm depth) for PDX survival study. Female C57BL/6 mice (Charles River, Wilmington, MA, USA) were implanted with 3×10^5 GL-261-LUC cells for syngeneic in vivo models. For all procedures, mice heads were fixed using a stereotaxic frame (David Kopf Instruments, Tujunga, CA, USA) under 2.5% isoflurane anesthesia (SomnoSuite, Kent Scientific, Torrington, CT, USA).

Chemotherapy and ionizing radiation (IR) therapy

For animal experiments, TMZ (Sigma, St Louis, MO, USA) was administered intraperitoneally (IP) at 5 mg/kg (the equivalent of 20% of the full therapeutic dose)[30,49]. For in vitro work, the stock solution of TMZ was diluted in media. Irradiation was performed using an XRAD 320 small animal irradiator (Precision X-ray Inc., Madison, CT, USA, delivery rate: 1.2 Gy/min) at Mount Sinai and Mark I Cs-137 Irradiator (J.L. Shepherd & Associates, San Fernando, CA, USA, delivery rate: 2.81 Gy/min) at the University of Pittsburgh. For animal irradiation, mice were restrained in DecapiCones (BrainTree Scientific, Braintree, MA) and placed in a custom-built lead shield to expose only their heads. Two fractions of radiation were administered for all in vivo studies.

In vitro water bath hyperthermia (HT)

Water bath HT was performed in vitro using a heated circulating water bath (Julabo, Allentown, PA, USA). Briefly, water bath HT involves immersing a flask containing cells into pre-heated water without the use of nanoparticles. Although MHT has been shown to be 16% more efficient in cytotoxic effects compared to water bath HT[50], water bath HT was chosen over MHT as MIONPs' optical properties may interfere with cell viability assays and high iron concentrations can induce ferroptosis, potentially obscuring heat treatment effects. Moreover, the most important factor for in vitro HT is the thermal dose (a product of temperature and time of exposure), which is independent of the heating method[51]. Therefore, water bath HT allowed us to better isolate the effects of heat on cancer cell proliferation and viability. A more detailed description of this protocol has been previously published[52].

CellTiter GLO viability assay

Cell viability assays were performed following exposure to water bath hyperthermia, TMZ, and/or ionizing radiation (IR). Cells were plated at 5×10^4 cells/well in black opaque 96-well plates (Thermo) and incubated for 72 h (SD3) or 120 h (G-16032, GL-261). CellTiter GLO assay (Promega, Madison, WI, USA) was performed per manufacturer's protocol and luminescence was measured using an Infinite M1000 PRO microplate reader (Tecan, Männedorf, Switzerland) and Magellan V7.2 software (Tecan). Exposure concentrations were determined based on separate monotherapy dose-escalation studies (Supplementary Fig. 4), selecting doses that reduced cell viability by approximately 10–30% compared to untreated controls.

Evaluating the synergistic, additive, or antagonistic effects of hyperthermia in combination with radiation or chemotherapy in glioblastoma cell lines

SD3 and GL-261 GBM cells were exposed to escalating doses of IR or TMZ with or without water bath hyperthermia pre-treatment to further characterize the combinatory effects of HT with TMZ or IR. Cell viability was assessed using CellTiter-GLO following dose escalation of HT monotherapy, TMZ or IR alone, and TMZ or IR after HT pre-treatment at a fixed dose. Combination index (CI) and dose-reduction index (DRI) were then calculated using the CompuSyn software, which employs the median-effect principle of mass-action law to assess combination effects described by the original Chou-Talalay method[53,54]. CI values were interpreted based on guidelines provided by Chou et al.[22] CI < 0.1 (very strong synergism), 0.1–0.3 (strong synergism), 0.3–0.7 (synergism), 0.7–0.85 (moderate synergism), 0.85–0.9 (slight synergism), 0.9–1.1 (nearly additive), 1.1–1.2 (slight antagonism), 1.20–1.45 (moderate antagonism), 1.45–3.3 (antagonism), 3.3–10 (strong antagonism), > 10 (very strong antagonism).

Clonogenic survival assays

GL-261 cells were plated in triplicate onto 10 cm cell-culture dishes (Corning Inc., Corning, NY, USA) after exposure to water bath hyperthermia, TMZ, and/or IR. Clonogenic survival assay was performed using methods previously described[55]. Cell seeding densities: Untreated – 1×10^3; Single-agent exposure (HT, TMZ or IR alone) – 3×10^3; Dual-agent exposure (TMZ + IR, HT + TMZ, or HT + IR) – 7.5×10^3; Triple-agent exposure (HT + TMZ + IR) – 1×10^4. Clonogenic assay was not possible with SD3 or G-16,302 as neither formed distinct, countable colonies.

AnnexinV/Propidium iodide assay and flow cytometry

SD3 or GL-261 GBM cells were seeded at a density of 1×10^5 in a 12-well plate in their culturing media. One day after seeding, cells were treated with HT (SD3: 43.5 °C for 20 min; GL261: 43.5 °C for 30 min), CRT (SD3: 6.5 μm + 2.8 Gy; GL261: 37.5 μm + 3 Gy), HT + CRT (SD3: 43.5 °C for 20 min + 6.5 μm + 2.8 Gy; GL261: 43.5 °C for 30 min + 37.5 μm + 3 Gy). Cells were incubated for 4–24 h and then samples were collected and stained with AnnexinV/Propidium iodide kit (Annexin V apoptosis detection kit, 88-8005-72, eBioscienceTM, Thermo Fisher) following manufacturer instructions. Samples were analyzed by Flow Cytometry (LSRFortessaTM Cell Analyzer, BD Biosciences, Franklin Lakes, NJ) within 4 h. Flow cytometry analysis were performed using FlowJo Software (Tree Star Inc. Ashland, OR, USA).

Magnetic iron oxide nanoparticles (MIONPs)

Synomag® MIONPs (Micromod Partikeltechnologie, GmbH, Rostock, Germany) are commercially available nanoflower-type maghemite (γ-Fe$_2$O$_3$) nanoparticles. Their synthesis and physical characterization have been previously described[56,57]. MIONPs used for the described studies were custom-prepared by the manufacturer to have a carboxylic acid surface coating and a hydrodynamic diameter of 50 nm, suspended in sterile water with an iron concentration of 80 mg/mL. They were used as received. Prior to in vivo use, their heating profile was characterized via test-tube calorimetry measurements, and the specific loss power – a measure of heating efficiency – was calculated (Supplementary Figs. 2, 5, 6).[58]

Convection-enhanced delivery (CED) of MIONPs

A Hamilton microliter syringe (Model 1705 SN) was pre-filled with MIONPs, and the needle was guided using the same coordinates as for tumor implantation. The syringe was fitted into a hydraulic pump apparatus connected to a digital pump controller (UltraMicroPump II; World Precision Instruments Inc., Sarasota, FL, USA). MIONPs were then delivered at an infusion rate of 0.5 μL/min based on prior CED studies[17,21]. Validation of localized intracranial delivery of MIONPs via CED in the rodent brain was confirmed via MicroPET CT prior to all treatments with MHT. Intracranial presence of MIONPs was further confirmed via MPI (Supplementary Fig. 3).

Rodent MHT

The AMF generator used for MHT was the D5 series G2 Driver (nanoScale Biomagnetics, Zaragoza, Spain), which included three different field generating coils that could be interchanged for application of MHT to rodents, cells, or for test-tube calorimetry measurements of MIONPs. Additional information regarding this system can be found in supplementary methods. Each animal was placed in a prone position on a plastic bed within the G2 driver AMF generator with their head between the two coils of the double H CoilSet. The AMF was applied for the duration of treatment after selection of the desired field frequency and amplitude. A visual representation is provided in Fig. 3A-B.

MHT intracranial thermometry

Intracranial temperature measurements were performed on non-tumor bearing C57BL/6 mice following CED of MIONPs. After CED, a guide cannula (PlasticsOne, Roanoke, VA, USA) was surgically implanted into the same burr hole used for CED. A fiber optic temperature probe (Neoptix, Burnaby, BC, Canada) connected to the D5 series G2 driver was then inserted through the canula, reaching a depth of 3 mm beneath the skull for continuous thermometry. MHT was performed as described. A visual representation is provided in Fig. 3C.

Bioluminescence imaging (BLI) and tumor burden assessment following MHT in combination with CRT

C57BL/6 mice were implanted with 3×10^5 GL-261-LUC GBM cells each and divided into four groups (untreated, CRT alone, MHT alone, MHT + CRT, $n = 5$ per group). Mice were randomized based on tumor size from BLI images 6 days post-implantation. BLI was performed using the IVIS Lumina XR in vivo imaging system (Perkin Elmer). 15 mg/mL D-luciferin (Perkin Elmer) was injected IP at a dose of 150 mg/kg. 7 min after luciferin injection, images were acquired every minute for a total of 10 min. Conditions for image acquisition: exposure time: 1 min; field of view: D; binning: medium; f/stop = 1. ROIs of the ten time points were analyzed with the Living Image 4.3 software and the 10 measurements per mouse were exported into an Excel file with the highest average radiance for each mouse used for subsequent analysis.

Human GBM PDX survival study

Brains of athymic nude mice were implanted as described above with 5×10^5 SD3 human GBM cells each and randomly assigned into one of four groups (untreated, CRT alone, MHT alone, MHT + CRT, $n = 10$ per group).

Magnetic resonance imaging (MRI) and computerized tomography (CT)

MRI A Bruker 9.4 Tesla 89-mm bore MRI system at the Icahn School of Medicine and 7 T MRI Scanner at the UPMC Hillman Cancer Center (Bruker, Carteret, NJ) with a 20-centimeter (cm) bore were used for high-resolution imaging of the rodent brain. T2-weighted coronal images of the rodent brain were obtained for tumor growth confirmation.

PET-CT The nanoScan Micro PET/CT (Mediso, Budapest, Hungary) at the Icahn School of Medicine and Siemens Inveon small animal PET-CT (Malvern, PA) at UPMC were used to obtain coronal images for visualization of MIONPs.

Immunofluorescence and staining

Brains of C57BL/6 mice were implanted as described with 3×10^5 GL-261-LUC cells per mouse and divided into three treatment groups: untreated control ($n = 3$), CRT alone (5 Gy x 2, 5 mg/kg x 2 TMZ), and MHT + CRT ($n = 4$ each). For the CRT alone group, sample sizes varied by analysis: $n = 3$ for γ-H2AX and HSP90, and $n = 4$ for CD4, CD8, and IBA-1 assessments. Coronal cryosections (14 μm) were prepared and incubated with primary antibodies: rabbit anti-γH2AX (1:500, 9718 S, Cell Signaling Technology, Danvers, MA), mouse anti-HSP90 (1:50, AB13492, Abcam, Cambridge, UK), mouse anti-CD4 (1:800, 67786, Proteintech, Rosemont, IL), rabbit anti-CD8 (1:800, AB217344, Abcam), rabbit anti-CD25 (1:800, CST, 39475 S), rat anti-Foxp3 (1:100, Invitrogen, 14-5773-82), and mouse anti-IBA1 (1:200, AB283319, Abcam). Sections were incubated with secondary antibodies: Alexa 594 goat anti-rabbit IgG (H + L) and Alexa 488 goat anti-mouse IgG (H + L), all used at 1:200 (Invitrogen, Thermo Fisher). Fluorescent images were acquired using an Olympus VS200 Research Slide Scanner (Olympus, Tokyo, Japan). γ-H2AX was quantified in the tumor area, while HSP90, CD4, CD8, and IBA-1 were quantified in the entire treated hemisphere, as these markers were expressed intra- and peri-tumorally.

Statistical analysis

GraphPad Prism version 10.1.1 (GraphPad Software, Boston, MA) was used for all graphing and statistical analysis. Student *t* test, Tukey's multiple comparison test, and 1- or 2-way ANOVA were used, as appropriate, to calculate statistical significance of data obtained from cell culture, tumor burden, and imaging studies. Kaplan–

Meier survival analyses of mouse cohorts was performed using the Log-rank Mantel Cox test. For all graphs, P values indicating level of significance are described in the figure legend.

Data availability

All data generated in this study are presented in this manuscript and supplementary materials will be publicly available upon publication of these findings. Requests for data can be sent to Dr. Constantinos Hadjipanayis (hadjipanayiscg2@upmc.edu).

References

1. Ostrom, Q. T., Cioffi, G., Waite, K., Kruchko, C. & Barnholtz-Sloan, J. S. CBTRUS statistical report: Primary brain and other central nervous system tumors diagnosed in the United States in 2014–2018. *Neuro Oncol.* **23** iii1–iii105. https://doi.org/10.1093/neuonc/noab200 (2021).
2. Dymova, M. A., Kuligina, E. V. & Richter, V. A. Molecular mechanisms of drug resistance in glioblastoma. *Int. J. Mol. Sci.* https://doi.org/10.3390/ijms22126385 (2021).
3. Stupp, R. et al. Radiotherapy plus concomitant and adjuvant temozolomide for glioblastoma. *N Engl. J. Med.* **352**, 987–996. https://doi.org/10.1056/NEJMoa043330 (2005).
4. Vehlow, A. & Cordes, N. DDR1 (discoidin domain receptor tyrosine kinase 1) drives glioblastoma therapy resistance by modulating autophagy. *Autophagy* **15**, 1487–1488. https://doi.org/10.1080/15548627.2019.1618540 (2019).
5. Arvanitis, C. D., Ferraro, G. B. & Jain, R. K. The blood-brain barrier and blood-tumour barrier in brain tumours and metastases. *Nat. Rev. Cancer.* **20**, 26–41. https://doi.org/10.1038/s41568-019-0205-x (2020).
6. Venkataramani, V. et al. Glioblastoma hijacks neuronal mechanisms for brain invasion. *Cell* **185**, 2899–2917e2831. https://doi.org/10.1016/j.cell.2022.06.054 (2022).
7. van Solinge, T. S., Nieland, L., Chiocca, E. A. & Broekman, M. L. D. Advances in local therapy for glioblastoma—Taking the fight to the tumour. *Nat. Reviews Neurol.* **18**, 221–236. https://doi.org/10.1038/s41582-022-00621-0 (2022).
8. Dennis, C. L. & Ivkov, R. Physics of heat generation using magnetic nanoparticles for hyperthermia. *Int. J. Hyperth.* **29**, 715–729. https://doi.org/10.3109/02656736.2013.836758 (2013).
9. Gilchrist, R. K. et al. Selective inductive heating of lymph nodes. *Ann. Surg.* **146**, 596–606. https://doi.org/10.1097/00000658-195710000-00007 (1957).
10. Jain, T. K., Reddy, M. K., Morales, M. A., Leslie-Pelecky, D. L. & Labhasetwar, V. Biodistribution, clearance, and biocompatibility of iron oxide magnetic nanoparticles in rats. *Mol. Pharm.* **5**, 316–327. https://doi.org/10.1021/mp7001285 (2008).
11. Wankhede, M., Bouras, A., Kaluzova, M. & Hadjipanayis, C. G. Magnetic nanoparticles: An emerging technology for malignant brain tumor imaging and therapy. *Expert Rev. Clin. Pharmacol.* **5**, 173–186. https://doi.org/10.1586/ecp.12.1 (2012).
12. Kalamida, D. et al. Fever-range hyperthermia vs. hypothermia effect on cancer cell viability, proliferation and HSP90 expression. *PLoS One.* **10**, e0116021. https://doi.org/10.1371/journal.pone.0116021 (2015).
13. Moon, S. D. et al. Definitive radiotherapy plus regional hyperthermia with or without chemotherapy for superior sulcus tumors: A 20-year, single center experience. *Lung Cancer.* **71**, 338–343. https://doi.org/10.1016/j.lungcan.2010.06.007 (2011).
14. den Brok, M. H. et al. In situ tumor ablation creates an antigen source for the generation of antitumor immunity. *Cancer Res.* **64**, 4024–4029. https://doi.org/10.1158/0008-5472.Can-03-3949 (2004).
15. Man, J. et al. Hyperthermia sensitizes glioma stem-like cells to radiation by inhibiting AKT signaling. *Cancer Res.* **75**, 1760–1769. https://doi.org/10.1158/0008-5472.CAN-14-3621 (2015).
16. Kaluzova, M., Bouras, A., Machaidze, R. & Hadjipanayis, C. G. Targeted therapy of glioblastoma stem-like cells and tumor non-stem cells using cetuximab-conjugated iron-oxide nanoparticles. *Oncotarget* **6**, 8788–8806. https://doi.org/10.18632/oncotarget.3554 (2015).
17. Platt, S. et al. Canine model of convection-enhanced delivery of cetuximab-conjugated iron-oxide nanoparticles monitored with magnetic resonance imaging. *Clin. Neurosurg.* **59**, 107–113. https://doi.org/10.1227/NEU.0b013e31826989ef (2012).
18. Maier-Hauff, K. et al. Efficacy and safety of intratumoral thermotherapy using magnetic iron-oxide nanoparticles combined with external beam radiotherapy on patients with recurrent glioblastoma multiforme. *J. Neurooncol.* **103**, 317–324. https://doi.org/10.1007/s11060-010-0389-0 (2011).
19. Yi, G. Q., Gu, B. & Chen, L. K. The safety and efficacy of magnetic nano-iron hyperthermia therapy on rat brain glioma. *Tumour Biol.* **35**, 2445–2449. https://doi.org/10.1007/s13277-013-1324-8 (2014).
20. Jordan, A. et al. The effect of thermotherapy using magnetic nanoparticles on rat malignant glioma. *J. Neurooncol.* **78**, 7–14. https://doi.org/10.1007/s11060-005-9059-z (2006).
21. Freeman, A. C. et al. Convection-enhanced delivery of cetuximab conjugated iron-oxide nanoparticles for treatment of spontaneous canine intracranial gliomas. *J. Neurooncol.* **137**, 653–663. https://doi.org/10.1007/s11060-018-2764-1 (2018).
22. Chou, T. C. Theoretical basis, experimental design, and clinical simulation of synergism and antagonism in drug combination studies. *Pharmacol. Rev.* **58**, 621–681. https://doi.org/10.1124/pr.58.3.10 (2006).
23. Rivera, D. et al. Neurosurgical applications of magnetic hyperthermia therapy. *Neurosurg. Clin. N Am.* **34**, 269–283. https://doi.org/10.1016/j.nec.2022.11.004 (2023).
24. Mahmoudi, K., Bouras, A., Bozec, D., Ivkov, R. & Hadjipanayis, C. Magnetic hyperthermia therapy for the treatment of glioblastoma: A review of the therapy's history, efficacy and application in humans. *Int. J. Hyperth.* **34**, 1316–1328. https://doi.org/10.1080/02656736.2018.1430867 (2018).
25. Borchers, J. et al. Magnetic anisotropy dominates over physical and magnetic structure in performance of magnetic nanoflowers. *Small Struct.* https://doi.org/10.1002/sstr.202400410 (2025).
26. Carlton, H. et al. Ranking magnetic colloid performance for magnetic particle imaging and magnetic particle hyperthermia. *Adv. Funct. Mater.* **35** 2412321 https://doi.org/10.1002/adfm.202412321 (2025).
27. Hainfeld, J. F. et al. Gold nanoparticle hyperthermia reduces radiotherapy dose. *Nanomedicine* **10**, 1609–1617. https://doi.org/10.1016/j.nano.2014.05.006 (2014).
28. Murad, H., Alghamian, Y., Aljapawe, A. & Madania, A. Effects of ionizing radiation on the viability and proliferative behavior of the human glioblastoma T98G cell line. *BMC Res. Notes.* **11**, 330. https://doi.org/10.1186/s13104-018-3438-y (2018).
29. Xu, Y., Hu, W. & Zhou, Q. Role of heat shock protein in radiation-induced effect and related potential clinical application. *Radiat. Med. Prot.* **6**, 51–60. https://doi.org/10.1016/j.radmp.2024.11.002 (2025).
30. Hadjipanayis, C. G., Fellows-Mayle, W. & Deluca, N. A. Therapeutic efficacy of a herpes simplex virus with radiation or temozolomide for intracranial glioblastoma after convection-enhanced delivery. *Mol. Ther.* **16**, 1783–1788. https://doi.org/10.1038/mt.2008.185 (2008).
31. Wang, H. Y., Fu, J. C., Lee, Y. C. & Lu, P. J. Hyperthermia stress activates heat shock protein expression via propyl isomerase 1 regulation with heat shock factor 1. *Mol. Cell. Biol.* **33**, 4889–4899. https://doi.org/10.1128/mcb.00475-13 (2013).

32. Whitesell, L. & Lindquist, S. L. HSP90 and the chaperoning of cancer. *Nat. Rev. Cancer.* **5**, 761–772. https://doi.org/10.1038/nrc1716 (2005).
33. Birbo, B., Madu, E. E., Madu, C. O., Jain, A. & Lu, Y. Role of HSP90 in cancer. *Int. J. Mol. Sci.* https://doi.org/10.3390/ijms221910317 (2021).
34. Orth, M. et al. Inhibition of HSP90 as a strategy to radiosensitize glioblastoma: Targeting the DNA damage response and beyond. *Front. Oncol.* https://doi.org/10.3389/fonc.2021.612354 (2021).
35. Vriend, L. E. M. et al. Boosting the effects of hyperthermia-based anticancer treatments by HSP90 Inhibition. *Oncotarget* **8**, 97490–97503. https://doi.org/10.18632/oncotarget.22142 (2017).
36. Chatenoud, L. in *Suppression and Regulation of Immune Responses: Methods and Protocols* (eds Maria Cristina Cuturi & Ignacio Anegon) 3–13 (Humana Press, 2011).
37. Li, Z., Deng, J., Sun, J. & Ma, Y. Hyperthermia targeting the tumor microenvironment facilitates immune checkpoint inhibitors. *Front. Immunol.* https://doi.org/10.3389/fimmu.2020.595207 (2020).
38. Antonios, J. P. et al. Immunosuppressive tumor-infiltrating myeloid cells mediate adaptive immune resistance via a PD-1/PD-L1 mechanism in glioblastoma. *Neuro Oncol.* **19**, 796–807. https://doi.org/10.1093/neuonc/now287 (2017).
39. Lim, M., Xia, Y., Bettegowda, C. & Weller, M. Current state of immunotherapy for glioblastoma. *Nat. Rev. Clin. Oncol.* **15**, 422–442. https://doi.org/10.1038/s41571-018-0003-5 (2018).
40. Rego, G. N. A. et al. Therapeutic efficiency of multiple applications of magnetic hyperthermia technique in glioblastoma using aminosilane coated iron oxide nanoparticles: In vitro and in vivo study. *Int. J. Mol. Sci.* **21**, 958 (2020).
41. Jordan, A. et al. Hyperthermia classic commentary: 'Inductive heating of ferrimagnetic particles and magnetic fluids: Physical evaluation of their potential for hyperthermia' by Andreas Jordan et al., International Journal of Hyperthermia, 1993;9:51–68 *Int. J. Hyperth* **25** 512–516. (2009). https://doi.org/10.3109/02656730903183445
42. Healy, S. et al. Clinical magnetic hyperthermia requires integrated magnetic particle imaging. *Wiley Interdiscip Rev. Nanomed. Nanobiotechnol.* **14**, e1779. https://doi.org/10.1002/wnan.1779 (2022).
43. D'Amico, R. S., Aghi, M. K., Vogelbaum, M. A. & Bruce, J. N. Convection-enhanced drug delivery for glioblastoma: A review. *J. Neurooncol.* **151**, 415–427. https://doi.org/10.1007/s11060-020-03408-9 (2021).
44. Huang, Y. et al. Plexin-B2 facilitates glioblastoma infiltration by modulating cell biomechanics. *Commun. Biol.* **4**, 145. https://doi.org/10.1038/s42003-021-01667-4 (2021).
45. Barrette, A. M. et al. Anti-invasive efficacy and survival benefit of the YAP-TEAD inhibitor verteporfin in preclinical glioblastoma models. *Neuro Oncol.* **24**, 694–707. https://doi.org/10.1093/neuonc/noab244 (2022).
46. Umphlett, M. et al. Widely metastatic glioblastoma with BRCA1 and ARID1A mutations: A case report. *BMC Cancer.* **20**, 47. https://doi.org/10.1186/s12885-020-6540-1 (2020).
47. Xie, X. P. et al. Quiescent human glioblastoma cancer stem cells drive tumor initiation, expansion, and recurrence following chemotherapy. *Dev. Cell* **57**, 32–46.e38 (2022). https://doi.org/10.1016/j.devcel.2021.12.007
48. Bozec, D. et al. Akaluc bioluminescence offers superior sensitivity to track in vivo glioma expansion. *Neurooncol Adv.* **2**, vdaa134. https://doi.org/10.1093/noajnl/vdaa134 (2020).
49. Aghi, M., Rabkin, S. & Martuza, R. L. Effect of Chemotherapy-Induced DNA repair on oncolytic herpes simplex viral replication. *JNCI: J. Natl. Cancer Inst.* **98**, 38–50. https://doi.org/10.1093/jnci/djj003 (2006).
50. Herea, D. D. et al. Comparative effects of magnetic and water-based hyperthermia treatments on human osteosarcoma cells. *Int. J. Nanomed.* **13**, 5743–5751. https://doi.org/10.2147/ijn.S174853 (2018).
51. Chamani, F., Barnett, I., Pyle, M., Shrestha, T. & Prakash, P. A. Review of in vitro instrumentation platforms for evaluating thermal therapies in experimental cell culture models. *Crit. Rev. Biomed. Eng.* **50**, 39–67. https://doi.org/10.1615/CritRevBiomedEng.2022043455 (2022).
52. Sharma, A. et al. Increased uptake of doxorubicin by cells undergoing heat stress does not explain its synergistic cytotoxicity with hyperthermia. *Int. J. Hyperth.* **36**, 712–720. https://doi.org/10.1080/02656736.2019.1631494 (2019).
53. Chou, T. C. & Talalay, P. Quantitative analysis of dose-effect relationships: The combined effects of multiple drugs or enzyme inhibitors. *Adv. Enzyme Regul.* **22**, 27–55. https://doi.org/10.1016/0065-2571(84)90007-4 (1984).
54. Chou, T. & Martin, N. CompuSyn for drug combinations: PC software and user's guide: A computer program for quantitation of synergism and antagonism in drug combinations, and the determination of IC50 and ED50 and LD50 values. *ComboSyn, Paramus, NJ* (2005).
55. Franken, N. A. P., Rodermond, H. M., Stap, J., Haveman, J. & van Bree, C. Clonogenic assay of cells in vitro. *Nat. Protoc.* **1**, 2315–2319. https://doi.org/10.1038/nprot.2006.339 (2006).
56. Gavilán, H. et al. Colloidal flower-shaped iron oxide nanoparticles: Synthesis strategies and coatings. *Part. Part. Syst. Charact.* **34**, 1700094. https://doi.org/10.1002/ppsc.201700094 (2017).
57. Bender, P. et al. Relating magnetic properties and high hyperthermia performance of iron oxide nanoflowers. *J. Phys. Chem. C.* **122**, 3068–3077. https://doi.org/10.1021/acs.jpcc.7b11255 (2018).
58. Soetaert, F., Korangath, P., Serantes, D., Fiering, S. & Ivkov, R. Cancer therapy with iron oxide nanoparticles: Agents of thermal and immune therapies. *Adv. Drug Deliv. Rev.* **163–164**, 65–83. https://doi.org/10.1016/j.addr.2020.06.025 (2020).

Acknowledgements

Author contributions

Conception of the project – C.H., R.I.; Experimental design – D.R., A.B., M.M., M.A., I.J.; Data production and formal analysis – D.R., A.B., M.M., M.A., A.C.P., O.P., I.J., C.K., A.S., T.C., H.C.; Manuscript preparation – D.R., A.B.; Review & Editing – all authors; Project administration and funding acquisition – C.H., R.I.

Funding information

Declarations

Competing interests

C.H. is a paid consultant for Hemerion Therapeutics, Integra, Stryker Corp., Synaptive Medical, and True Digital Surgery, which have no relationship with the work presented in the manuscript. R.I. was a consultant and member of the Scientific Advisory Board of Imagion Biosystems, Ltd. through end of Dec 2023. This arrangement was reviewed and approved by the Johns Hopkins University in accordance with its conflict-of-interest policies. R.I. is an inventor listed on several nanoparticle patents. All patents are assigned to either The Johns Hopkins University or Aduro Biosciences, Inc. All other authors report no other conflicts of interest.

Additional information

Supplementary Information The online version contains supplementary material available at https://doi.org/10.1038/s41598-025-95544-3.

Correspondence and requests for materials should be addressed to C.G.H.

Reprints and permissions information is available at www.nature.com/reprints.

Publisher's note Springer Nature remains neutral with regard to jurisdictional claims in published maps and institutional affiliations.